Pitting Behavior of L415 Pipeline Steel in Simulated Leaching Liquid Environment

H.X. Wan, X.J. Yang, Z.Y. Liu, D.D. Song, C.W. Du, and X.G. Li

The corrosion behavior and laws of the west-east gas pressure pipeline of L415 steel were studied in simulated leaching liquid. The failure of the L415 steel during the pressure testing process was investigated using electrochemical polarization, electrochemical impedance spectroscopy, and immersion test. The corrosion rate of the L415 steel increased with ion concentration in the leaching liquid. This rate reached about 0.8 mm a^{-1} and belonged to the severe corrosion grade. Pitting corrosion was observed in various simulated solutions with different aggressive species concentrations. The original ion concentration in the leaching liquid (1×) is the key factor influencing pitting initiation and development. Pitting showed easy nucleation, and its growth rate was relatively slow, in the basic simulating solution of the leach liquid (i.e., the ion content is compactable to the real condition in the rust on the inner steel pipe surface). Pitting was also highly sensitive and easily grew in the solution with doubled ion concentration in the basic simulating solution (2×). A uniform corrosion, instead of pitting, mainly occurred when the ion concentration was up to 10× of the basic solution.

1. Introduction

The long-term security service of pipeline steel used in oil and gas transport is greatly significant in energy security and economic operations. The corrosion of high-strength pipeline steel, especially stress corrosion cracking (SCC), is one of the main threats for pipeline steel operation safety and life (Ref 1-3). The high-strength pipeline in the oil and gas transport process can cause SCC both in the internal and external environments. The internal pipeline SCC is mainly caused by hydrogen-induced cracking, which is caused by acid gases, such as (H_2S, CO_2) dissolved in tube effusion (Ref 4-6). Meanwhile, the external pipeline SCC is mainly caused by the corrosive medium in soil permeating into the coating. Many domestic and overseas SCC accidents have occurred in the past few decades. These accidents have led to huge economic losses (Ref 7-10). The high-strength pipeline steel services are very short in China, and no similar stress corrosion accidents have been reported. Bodies of research (Ref 11, 12) show that pitting corrosion is one of the major causes of crack initiation in the internal or external pipe SCC. Pitting generates high stress concentration effects, which can promote crack initiation and propagation, and promotes some corrosive substances, such as Cl^-. These substances are enriched in corrosion pits and result in acidification inside the pitting corrosion solution. All these conditions make the steel matrix suffer from rapid electrochemical dissolution in the crack tip position then the crack

extension (Ref 13-15). Pitting can also damage the integrity of steel pipes, which results in hole leakage.

This study uses a buried L415 steel pipe for nature gas transportation. This pipe has successively completed the water pressure, sweep water, and pressure maintaining work before being employed. The holding pressure by 80% N_2 and 20% O_2 lasting about 7-12 months is 4.5 MPa. After which, the server pitting corrosion, including several hole leakages, is found in the pipe within more than 20-km distance. The maximum pitting growth rate is 1.4 mm a^{-1}, and this phenomenon is rare in the corrosion case.

A preliminary analysis shows that the rapid corrosion perforation is related to the internal pipeline high-pressure and oxygen-enriched environment. The rust on the internal surface contains a concentrated corrosive medium, including Cl^-, SO_4^{2-}, and HCO_3^-. Under a humid condition, the corrosive environment will be formed in the rust, which would lead to severe pitting corrosion. The corrosion medium remaining in the rust layer will further promote the pitting initiation and growth, which may turn into pipeline steel SCC in the presence of intensive enough tensile stress, if the corrosive medium is not removed before the pipeline operation.

This study conducts the electrochemical polarization, electrochemical impedance spectroscopy, and immersion test combined with scanning electron microscopy (SEM) observation to investigate the pitting corrosion of the L415 pipeline carbon steel in the simulated leach condition of the rust layer. This research aims to better understand the pitting behavior and provide the basis for the establishment of relevant protective measures.

2. Experimental

2.1 Materials

All experiment samples were cut from the same piece of L415 buried pipeline steel for natural gas with the following chemical composition (wt.%): C 0.1, Si 0.22, Mn 1.22, P 0.012,

H.X. Wan, X.J. Yang, Z.Y. Liu, D.D. Song, C.W. Du, and X.G. Li, Corrosion and Protection Center, University of Science and Technology Beijing, Beijing 100083, China. Contact e-mail: liuzhiyong7804@126.com.

S 0.0033, Nb 0.028, Ni 0.032, Cr, Mo, Cu ≤ 0.01 and Fe balance.

2.2 Test Condition

The test solution was leach liquid from the rust layer, which was stranded in corrosion products after a holding pressure of 7-12 months in the liquid-phase environment. The ion concentration in the leaching liquid in corrosion products (mg L^{-1}) was F^- 7.135, Cl^- 54.890, SO_4^{2-} 204.015, NO_3^- 4.716, Na^+ 469.182, K^+ 28.846, Ca^{2+} 37.756, and Mg^{2+} 16.842. Following the law of charge and mass conservation of cationic and anionic ions, the principle of applying high concentration, instead of low concentration, was adopted to achieve balance. First, less complex ion was used followed by high content ions. The common chemical reagent was then used to configure the simulation solution. The simulated solution of the leaching liquid (g L^{-1}) $NaHCO_3$ 0.294, NaF 0.0157, $CaCl_2$ 0.0888, Na_2SO_4 0.213, KNO_3 0.091, $MgSO_4.7H_2O$ 0.172 was utilized with dilute hydrochloric acid solution having a pH adjusted to 4.5. The pitting corrosion of the L415 steel was studied in $1\times$, $2\times$, $5\times$, $10\times$, and $20\times$ ion concentrations placed in an autoclave and pressurized to 5 MPa with 80% N_2 + 20% O_2 to simulate the failure environment. In order to study the effect of O_2 on corrosion, 100% N_2 maintaining pressure was used in polarization curve testing. In this paper, the maintaining pressure all was 80% N_2 + 20% O_2 without special instructions. All solutions were analytical pure chemical reagents and deionized water.

2.3 Electrochemical Measurement

The electrochemical specimens measured 10 mm × 10 mm × 3 mm. The specimens were coated with an epoxy resin, which left an exposure face of 10 mm × 10 mm. The working face of the electrode was sequentially ground to 1500 grit emery paper and then cleaned using acetone. The electrochemical tests were conducted on a PARSTAT2273 electrochemical workstation with a three-electrode cell system, in which the specimens were used as the working electrode, Ag/AgCl as the reference electrode, and a platinum plate as the counter electrode. Prior to measurement, the working electrode was maintained for 30 min in the solution to ensure that a steady-state value of the corrosion potential was reached. The electrochemical impedance spectroscopy (EIS) was measured at the AC voltage disturbance of 10 mV, with a test frequency ranging from 100 kHz to 10 mHz. The potentiodynamic polarization curves were measured at a potential sweeping rate of 0.5 mV s^{-1} at a relatively open-circuit potential from -0.5 V (versus SCE) to 0.5 V (versus SCE).

2.4 Immersion Test

The immersion test measured 35 mm × 25 mm × 2 mm. The sample surfaces were burnished parallel to the tension direction to 800 grits before cleaning in distilled water and acetone. Three groups of parallel samples were used in each experimental condition. The vertical sample was suspended in the autoclave in different ion concentrations with 5 MPa high pressure using 80% N_2 +20% O_2. Pictures were taken with a camera before and after the experiment. After immersion for 10 and 30 days, the corrosion product that formed on the sample was thoroughly removed using a descaling solution that contained 500 mL of HCl (special gravity, 1.189), 500 mL of

distilled water, and 3.5 g of hexamethylenetetramine. L415 steel was weighed before immersing and after removing the corrosion product to study the corrosion rate by weightlessness in leaching liquid environment. The specimen morphology was observed using an asana microscope and SEM (Quanta 250) after rinsing and drying. The pitting morphology of L415 steel was observed by SEM after immersion, the depth of pitting of L415 steel was measured by asana microscope after immersion, and the growth rate of pitting was calculated by the data of pitting depth. All the experiments were conducted at room temperature ($\sim$22 °C).

3. Results

3.1 Electrochemical Measurements

Figure 1(a) shows the polarization curves of the L415 pipeline steel in the simulated leaching liquid environments. The anode polarizations were controlled by the active and cathode polarizations were controlled by diffusion in various ion concentration. The polarization curve shifted right, and the corrosion rate increased with the increase in the ion concentration. Figure 1(b) shows the polarization curves of the L415 pipeline steel in the simulated leaching liquid concentration pressured in 80% N_2 + 20% O_2 (failure environment) and 100% N_2. The result shows that the shape of two polarization curve in different pressure environment is similar, only the corrosion potential in N_2 pressure was shift negative. The corrosion potential and current density were fitted from Fig. 1 data in Table 1. The results of Table 1 showed that the corrosion current density of the L415 steel in the $1\times$ and $20\times$ leaching liquid environment was close to the 0.043 and 0.314 mA which shows the concentration in liquid leaching has a significant effect on the corrosion. The corrosion current density in $1\times$ leaching liquid concentration pressure in 80% N_2 + 20% O_2 (failure environment) and 100% N_2 was 0.043 and 0.041 mA cm^{-2}, respectively, and the corrosion current density was similar which shows that the O_2 in leaching liquid environment is not the main factors to affect corrosion.

Figure 2 shows the EIS of the L415 pipeline steel obtained under various ion concentrations in the leaching liquid. The Nyquist of the EIS of the L415 steel in different leaching liquids was roughly the same: only having one capacitive reactance arc. The low-frequency part of the capacitive reactance arc skewed left and had real component shrinkage, which showed an inductive arc. The capacitive reactance arc radius and low-frequency module value diminished with the increase in the ion concentration, which showed that the corrosion resistance reduced and the corrosion rate increased. These results were consistent with those of the polarization curve.

3.2 Surface Characterization

Figure 3 shows the surface morphologies of the L415 steel immersed in $1\times$, $2\times$, and $10\times$ leaching liquid ion concentrations after 10 and 30 days. The L415 pipeline steel produced much pitting in the simulated leaching liquid. The pitting corrosion of the L415 steel was more serious in the $1\times$ and $2\times$ leaching liquid than that in the $10\times$ leaching liquid regardless of the immersion duration (i.e., 10 or 30 days). The number of pitting was high. The depth was deeper. The number of pitting

increased and the pitting diameter increased with the extended immersing time. Pitting was a kind of local corrosion with concealed exterior and bigger destructiveness. Pitting often easily became a source of SCC and corrosion fatigue crack when the components were affected by stress corrosion. The depth of the pits was then measured by a stereo microscope.

Figure 4 shows the stereo microscope morphology of the L415 pipeline steel immersed in $1\times$, $2\times$, and $10\times$ leaching liquid environment for 10 and 30 days. The largest pitting depth was observed from the pitting corrosion region when the pit depth rate was similar to that in the statistics. The sever pitting of the L415 steel was produced in $1\times$ and $2\times$ leaching liquid environment. The average maximum depth rate of pitting reached up to 0.85 and 0.81 mm a^{-1} when immersed in $1\times$ and $2\times$ leaching liquid environment for 10 days. The average

maximum depth rate of pitting reached up to 0.59 and 0.78 mm a^{-1} when the L415 pipeline steel was immersed for 30 days. The depth and diameter of pitting seemed to have less variance when immersed in $1\times$ leaching liquid environment for 10 and 30 days (Fig. 4). These results indicated that pitting slowly grew after 10 days of immersion in the $1\times$ liquid leaching environment. However, pitting corrosion was sensitive and easily grew in the $2\times$ liquid leaching environment. The pitting depth was shallow after 10 and 30 days of immersion in the $10\times$ leach liquid, which may have been caused by uniform corrosion. Statistics showed that the pitting depth rate did not increase with ion concentration in the L415 steel in the leaching liquid (Fig. 5). Meanwhile, the corrosion rate (Fig. 6) increased to 0.784, 0.772, and 0.836 mm a^{-1} and belonged to the severe corrosion grade. This result further illustrated that the L415 steel had uniform corrosion in the $10\times$ leaching liquid environment. Pitting corrosion occurred in the medium of the special ion, such as oxidant and active anion in the solution. Some active anions, especially halogen ions, can destroy the
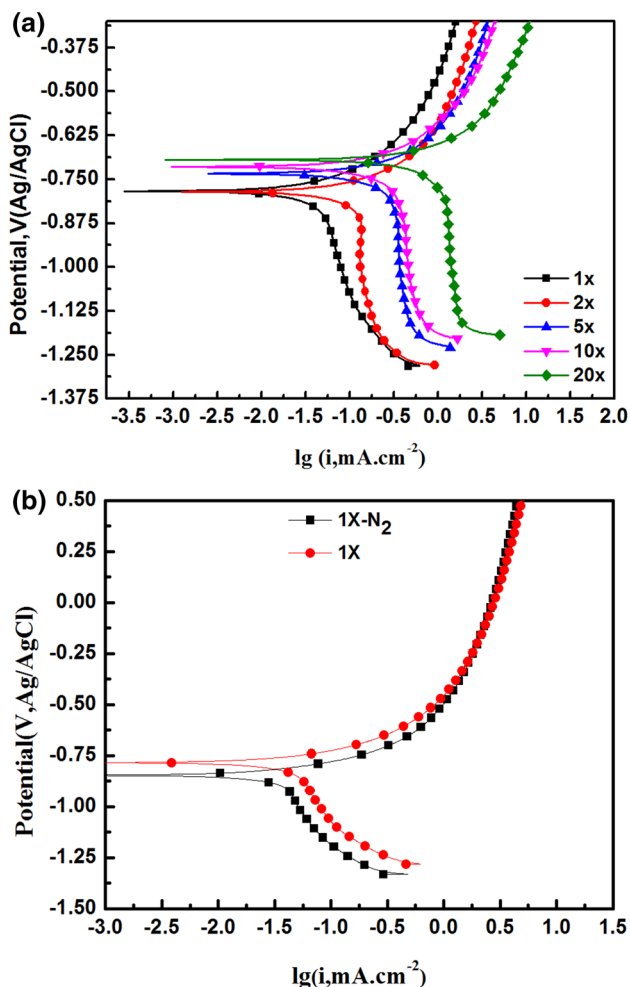

Fig. 1 Polarization curves of the L415 pipeline steel obtained under (a) various ion concentrations in the leaching liquid environment, (b) leaching liquid concentration in 100% N2 maintaining pressure
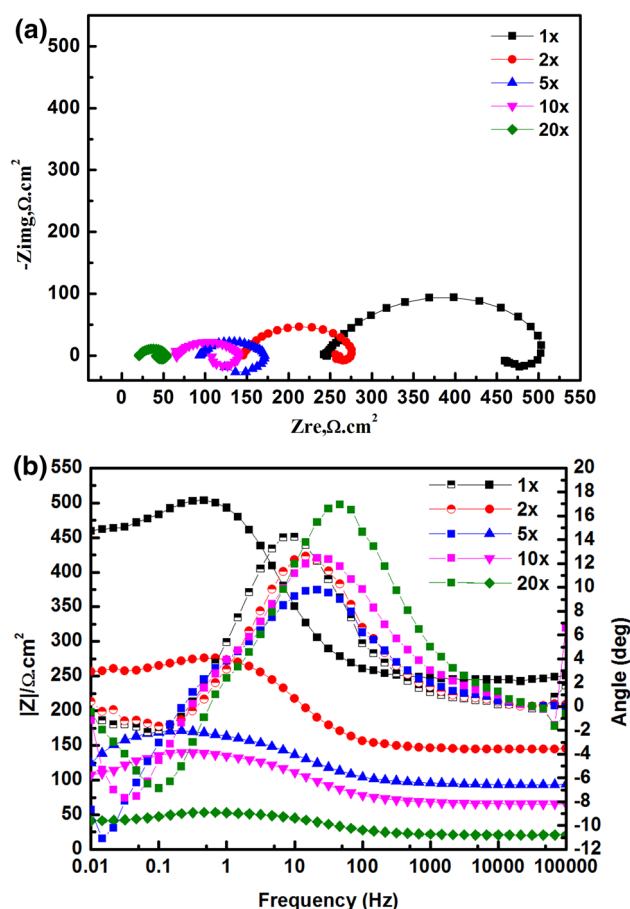

Fig. 2 EIS of the L415 pipeline steel under various concentrations of the leaching liquid (a) Nyquist; (b) bode

Table 1 Corrosion potential and current density of the L415 pipeline steel in simulated leaching liquid environments and leaching liquid concentration in 100% N$_2$ maintaining pressure

Ion concentration	$1\times$	$1\times$-N$_2$	$2\times$	$5\times$	$10\times$	$20\times$
E_{corr} (V)	−0.795	−0.844	−0.784	−0.733	−0.717	−0.713
I_{corr} (mA cm^{-2})	0.043	0.041	0.054	0.331	0.283	0.314
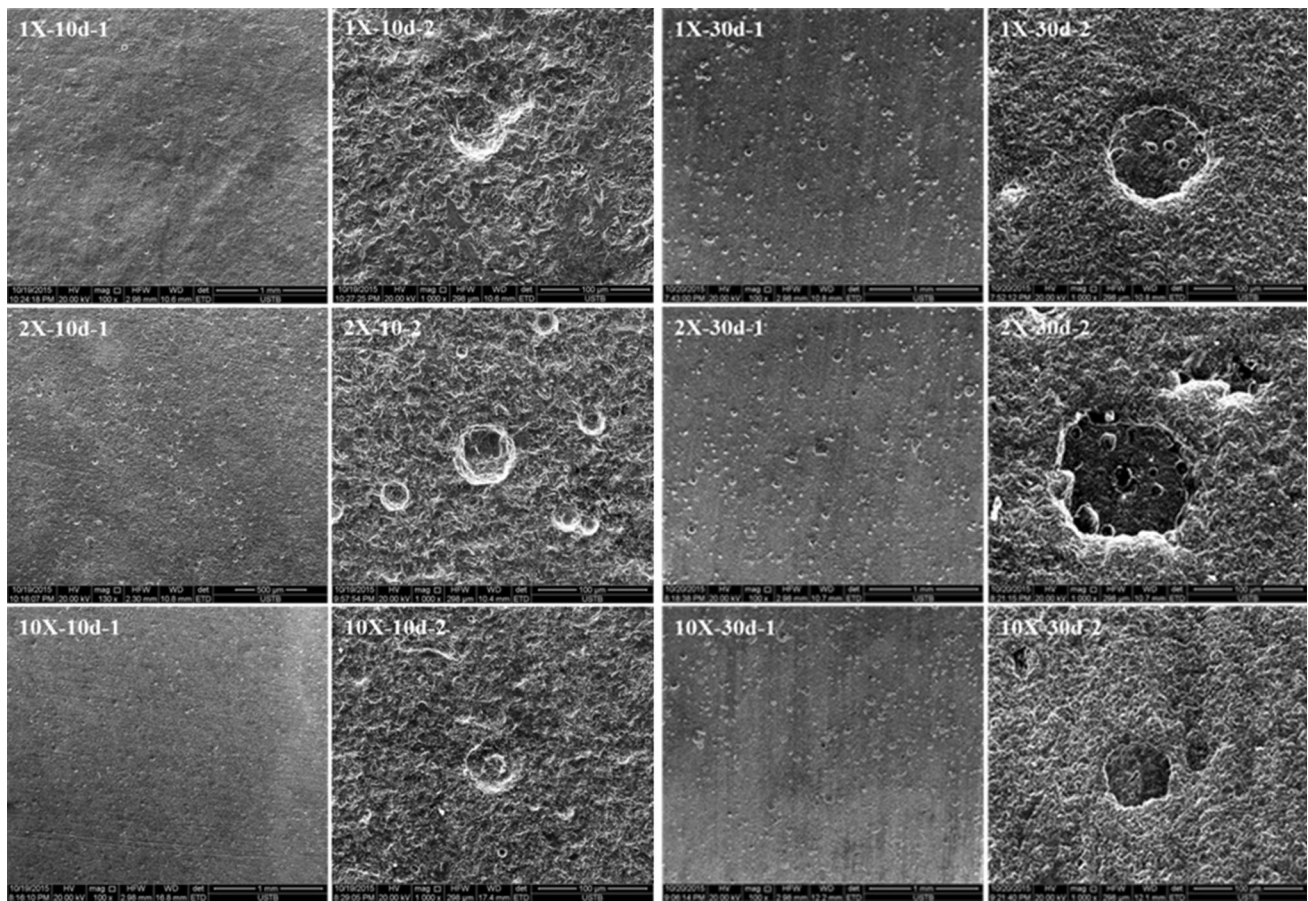
Fig. 3 Surface morphologies of the L415 steel immersed in ×1, ×2, and ×10 leaching liquid ion concentrations for 10 and 30 days

passivity of metals and cause pitting (e.g., Cl^- and SO_4^{2-}). Those special anions will not exhibit a uniform corrosion on the metal surface, which would lead to pitting. The research results (Ref 16) showed that pitting corrosion can occur when the Cl^- concentration reached 30 mg L^{-1}. The leaching liquid of the Cl^- concentration was as high as 55 mg L^{-1}. In addition, the SO_4^{2-} activity would also cause pitting. Therefore, the large amount of anion in the leaching liquid was the main cause of pitting corrosion. However, the density of the breakdown point of the corrosion product film largely increased and the continuous state was destroyed, which can lead the pitting nucleation to produce a uniform corrosion in the 10× leaching liquid environment when Cl^- increased to a high concentration.

3.3 XRD Corrosion Products Analysis

Figure 7 shows the XRD pattern of the corrosion product layer on the L415 pipeline steel after 30 days of immersion in the simulated solution with 1× and 2× leaching liquid. Visibly, the corrosion products were γ-FeOOH, Fe_2O_3, and Fe_3O_4. These Fe compounds can form a protective film, which slowed down the corrosion of the L415 steel. However, the volume of the Fe oxides will be larger when it formed a hydrate, which would lead to the loss of the corrosion product layer, and easily destroyed by Cl^- and SO_4^{2-}. The activation anode existed in locality, which can easily lead to pitting corrosion. From the XRD pattern, no obvious Fe carbonate was found in the corrosion products, which may be attributed to HCO_3^- existing in the form of an intermediate product and not existing in the
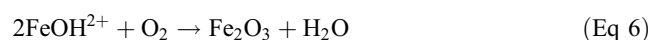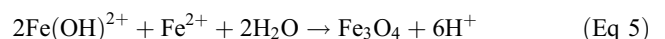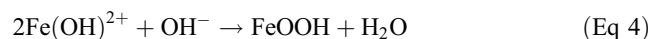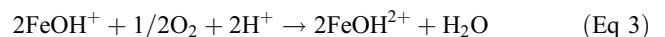
corrosion products, or few carbonate was generated, which the XRD cannot detect.

4. Discussion

The leaching liquid is an acidic environment. Hence, the following possibility electrochemical reactions are included:

$$Fe \rightarrow Fe^{2+} + 2e \qquad (Eq\ 1)$$

$$Fe^{2+} + H_2O \rightarrow FeOH^+ + H^+ \qquad (Eq\ 2)$$

The simulated leaching liquid is an oxygen-enriched environment, where Fe^{2+} and $FeOH^+$ are dissolved by oxygen oxidation:

$$2FeOH^+ + 1/2O_2 + 2H^+ \rightarrow 2FeOH^{2+} + H_2O \qquad (Eq\ 3)$$

$$2Fe(OH)^{2+} + OH^- \rightarrow FeOOH + H_2O \qquad (Eq\ 4)$$

$$2Fe(OH)^{2+} + Fe^{2+} + 2H_2O \rightarrow Fe_3O_4 + 6H^+ \qquad (Eq\ 5)$$

$$2FeOH^{2+} + O_2 \rightarrow Fe_2O_3 + H_2O \qquad (Eq\ 6)$$

At the beginning of the corrosion stage, Fe constantly exhibits anodic dissolution. The Fe^{2+} concentration in the reaction interface is higher. Therefore, a loose and porous corrosion product layer of the FeOOH membrane is formed on
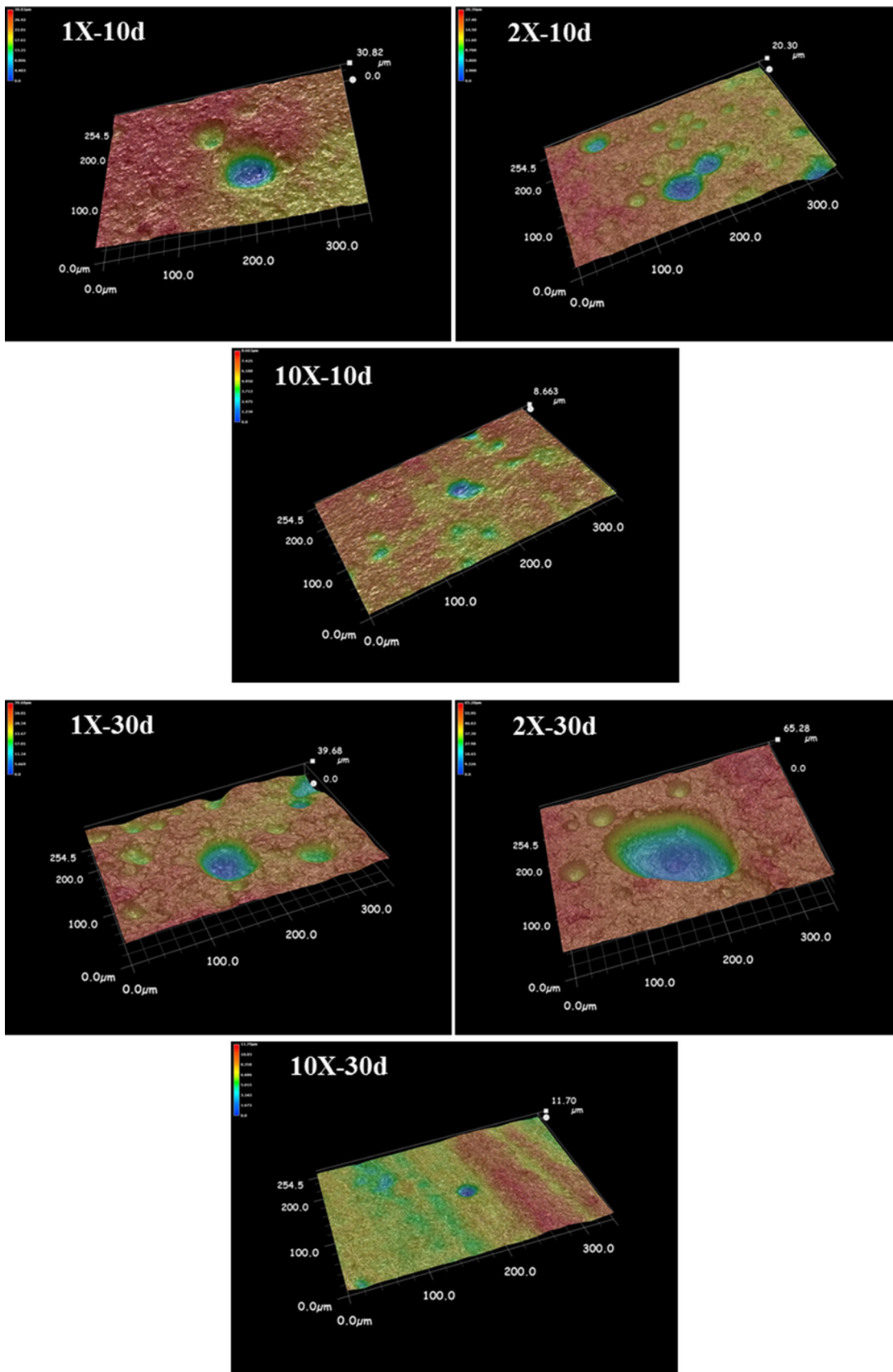
Fig. 4 Stereo microscope view of the L415 pipeline steel immersed in ×1, ×2, and ×10 leaching liquid environment for 10 and 30 days
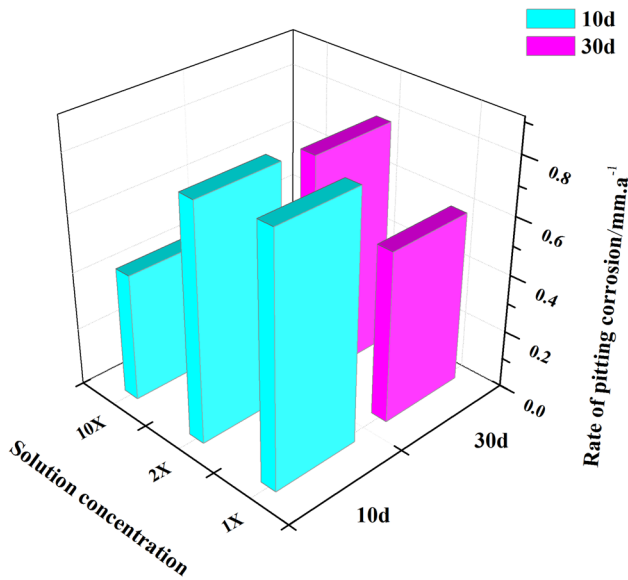
**Fig. 5** Average maximum pitting depth rate statistics of the L415 pipeline steel immersed in ×1, ×2, and ×10 leaching liquid environment for 10 and 30 days
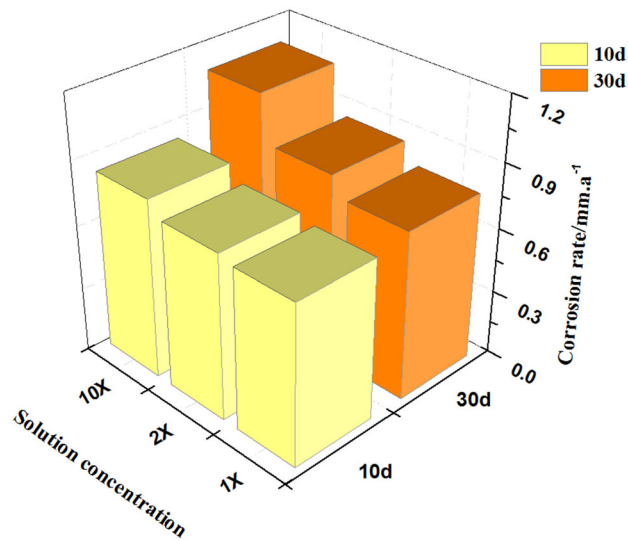
Fig. 6 Corrosion rate of the L415 pipeline steel immersed in ×1, ×2, and ×10 leaching liquid environment for 10 and 30 days

the electrode surface in a relatively short period of time. Forming the local activation point in space is easy. Cl^- and SO_4^{2-} would more easily enrich to anode activation nearby through these gap enrichments. The corrosion rate of the electrode increases, then pitting forms (Ref 17), which results in a local Cl^- gathering in the membrane and the destruction in the dynamic balance of the corrosion product film.

A mechanism analysis of pitting corrosion of the L415 steel in simulated leaching liquid is conducted.

The electrochemical results (Fig. 1 and 2) show that the L415 steel exhibits activation control in the simulated leaching liquid environment. The ion concentration increase would shift the polarization curve right, while the corrosion rate is accelerated. The concentration in liquid leaching has a significant effect on the corrosion. However, the O_2 in pressure was
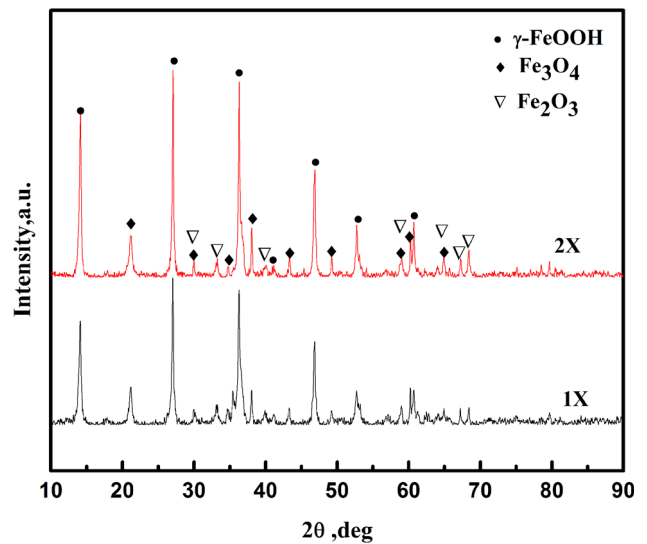
Fig. 7 XRD pattern of the corrosion product layer on the L415 pipeline steel after 30 days of immersion in the simulated solution with ×1 and ×2 leaching liquid

not the main factors to affect corrosion. The corrosion current density of the L415 steel reaches 0.043 mA cm^2 in the leaching liquid environment (failure environment) and belongs to the fast corrosion rate. The corrosion rate reaches about 0.8 mm a^{-1} and belongs to the severe corrosion grade. Moreover, the inductive loops in the low frequency (Fig. 2) indicate that the steel dissolution at this stage follows a consecutive mechanism with an intermediate product, probably $(FeOH)_{ads}$ adsorbed on the electrode surface. The corrosion scale initially formed is loose and non-protective. From the corrosion morphology, the destruction of the corrosion product film exhibits non-uniformity in a certain leaching liquid concentration, which often exists in the form of discontinuous activity points. In this case, the damage parts of the corrosion product film come to form the pitting nucleation. The pitting is rare and shallow in the sample surface when the ion concentration is 10× the leaching liquid (Fig. 3). The L415 pipeline generates a uniform corrosion when the ion concentration is high. Assume that the charge reaction resistance of the pitting area is R_{tp} and the surface charge of the non-pitting surface (with corrosion product film) for resistance is R_{tn}. R_{tp} and R_{tn} are the functions of the potential. The relationships are parallel with each other. The EIS performances of the capacitive reactance arc with a time constant in the high frequency and an inductance arc in low frequency are shown in Fig. 2.

Based on the abovementioned analysis, the charge transfer resistance R'_t of the electrode process is the apparent charge transfer resistance of the parallel R_{tn} and R_{tp}:

$$R'_t = \frac{R_{tn} \cdot R_{tp}}{R_{tn} + R_{tp}} \qquad \text{(Eq 7)}$$

The internal pitting surface is fresh metal, while the non-pitting surface is covered with corrosion products. Hence, $R_{tn} > R_{tp}$ must be satisfied if pitting occurs.

For the steady-state pitting, with the extended immersing time from t_1 to t_2, $R'_t(t)$ corresponds with time t, and $\Delta R'_t(t)$ is part of the charge of $R_{tn}(t)$ and $R_{tp}(t)$.

$\Delta R_{tn}(t)$ and $\Delta R_{tp}(t)$ can be, respectively, calculated as follows:

$$\Delta\left(\frac{1}{R_{tn}(t)}\right) = \Delta\left(\frac{1}{R_{tn}(t_2)}\right) - \Delta\left(\frac{1}{R_{tn}(t_1)}\right) \qquad \text{(Eq 8)}$$

$$\Delta\left(\frac{1}{R_{tp}(t)}\right) = \Delta\left(\frac{1}{R_{tp}(t_2)}\right) - \Delta\left(\frac{1}{R_{tp}(t_1)}\right) > 0 \qquad \text{(Eq 9)}$$

Therefore, according to Eq 7-9:

$$\Delta\left(\frac{1}{R'_t(t)}\right) = \Delta\left(\frac{1}{R_{tp}(t)}\right) - \left|\Delta\left(\frac{1}{R_{tn}(t)}\right)\right| \qquad \text{(Eq 10)}$$

The ability of the passivation substance in the medium to repair the corrosion product film is stronger [that can be set $\left|\Delta\left(\frac{1}{R_{tn}(t)}\right)\right| \approx 0$] if the corrosive medium concentration is low. The Cl^- aggregation in the nucleation zone of pitting can cause the increase of $\Delta\left(\frac{1}{R_{tp}(t)}\right)$, that is, the pitting corrosion can occur and R'_t decreases. The time for Cl^- to achieve a critical concentration for the stable growth of pitting will be relatively long when the Cl^- concentration is low. Therefore, the pitting density and size at lower concentration corrosion are smaller than those at the high concentration of the corrosive medium after the same time. Accordingly, the concentration increase will promote the pitting corrosion growth.

The destruction of the corrosion product film is discontinuous, and the corrosion point is the pitting nucleation if the protective layer of the corrosion product film is close and the corrosive ion concentration increases when the concentration of the corrosive ions (Cl^- and SO_4^{2-}) is low. However, gathering Cl^- together to reach a critical concentration and promote the pitting growth is difficult (Ref 18). The pitting nucleation is easy when the corrosion ion concentration is low. However, only a small part of the pitting can grow (Fig. 4). The corrosion product film is still in a continuous state, but $\Delta\left(\frac{1}{R_{tp}(t)}\right)$ greatly increases when the Cl^- concentration increases to the appropriate value. In this condition, the Cl^- concentration in pitting can easily reach a critical concentration to promote the rapid pitting growth. The pitting nucleation density is still low (Ref 19). In this case, the pitting growth significantly increases. The density of the breakdown corrosion product film greatly increases when the Cl^- concentration increases to a high value. The continuous state is further destroyed. The pitting nucleation is difficult when $\Delta\left(\frac{1}{R_{tp}(t)}\right) \approx 0$ and $\Delta\left(\frac{1}{R_{tn}(t)}\right) \geq 0$. A uniform corrosion, such as the result of the corrosion in the $10\times$ leaching liquid, also occurs.

5. Conclusion

1. With the increase in ion concentration in the leaching liquid, the polarization curve of the L415 steel moved right; the corrosion current density reached the 0.314 mA level; and the corrosion rate of the L415 steel reached about 0.8 mm a^{-1} in the leaching liquid that belongs to the severe corrosion grade.
2. The original ion concentration in the leaching liquid is the key factor influencing the pitting initiation and development. Pitting exhibits an easy nucleation and a relatively slow growth rate in the basic simulating solution of the leach liquid (i.e., the ion content is compactable to

the real condition in the rust on the inner steel pipe surface). Pitting corrosion is highly sensitive and easily grows in the solution with doubled ion concentration in the basic simulating solution. A uniform corrosion mainly occurs, instead of pitting, when the ion concentration is up to $10\times$ of the basic solution.

References

1. A. Fu and Y. Cheng, Electrochemical Polarization Behavior of X70 Steel in Thin Carbonate/Bicarbonate Solution Layers Trapped Under a Disbonded Coating and Its Implication on Pipeline SCC, *Corros. Sci.*, 2010, **52**(7), p 2511–2518
2. B. Saleem, F. Ahmed, M.A. Rafiq, M. Ajmal, and L. Ali, Stress Corrosion Failure of an X52 Grade Gas Pipeline, *Eng. Fail. Anal.*, 2014, **46**, p 157–165
3. S.S. Abedi, A. Abdolmaleki, and N. Adibi, Failure Analysis of SCC and SRB Induced Cracking of a Transmission Oil Products Pipeline, *Eng. Fail. Anal.*, 2007, **14**(1), p 250–261
4. I. Chattoraj, S. Tiwari, A.K. Ray, A. Mitra, and S.K. Das, Investigation on the Mechanical Degradation of a Steel Line Pipe Due to Hydrogen Ingress During Exposure to a Simulated Sour Environment, *Corros. Sci.*, 1995, **37**(6), p 885–896
5. G. Zhang, Y. Zeng, X. Guo, F. Jiang, D. Shi, and Z. Chen, Electrochemical Corrosion Behavior of Carbon Steel Under Dynamic High Pressure H_2S/CO_2 Environment, *Corros. Sci.*, 2012, **65**, p 37–47
6. P. Wang, J. Wang, S. Zheng, Y. Qi, M. Xiong, and Y. Zheng, Effect of H_2S/CO_2 Partial Pressure Ratio on the Tensile Properties of X80 Pipeline Steel, *Int. J. Hydrogen Energy*, 2015, **40**, p 11925–11930
7. M. Yan, C. Sun, J. Xu, T. Wu, S. Yang, and W. Ke, Stress Corrosion of Pipeline Steel Under Occluded Coating Disbondment in a Red Soil Environment, *Corros. Sci.*, 2015, **93**, p 27–38
8. Z. Liu, X. Li, C. Du, and Y. Cheng, Local Additional Potential Model for Effect of Strain Rate on SCC of Pipeline Steel in an Acidic Soil Solution, *Corros. Sci.*, 2009, **51**(12), p 2863–2871
9. B. Pan, X. Peng, W. Chu, Y. Su, and L. Qiao, Stress Corrosion Cracking of API, X-60 Pipeline in a Soil Containing Water, *Mater. Sci. Eng. A*, 2006, **434**(1), p 76–81
10. M. Yan, J. Wang, E. Han, and W. Ke, Local Environment Under Simulated Disbonded Coating on Steel Pipelines in Soil Solution, *Corros. Sci.*, 2008, **50**(5), p 1331–1339
11. S. Caines, F. Khan, and J. Shirokoff, Analysis of Pitting Corrosion on Steel Under Insulation in Marine Environments, *J. Loss Prev. Process Ind.*, 2013, **26**(6), p 1466–1483
12. M. Zhu, C. Du, X. Li, Z. Liu, H. Li, and D. Zhang, Effect of AC on Stress Corrosion Cracking Behavior and Mechanism of X80 Pipeline Steel in Carbonate/Bicarbonate Solution, *Corros. Sci.*, 2014, **87**, p 224–232
13. G. Van Boven, W. Chen, R. Rogge, and R. Sutherby, The Effect of Residual Stress on Pitting and Stress Corrosion Cracking of High Pressure Natural Gas Pipelines, *Acta Mater.*, 2007, **55**, p 29–43
14. A. Turnbull, S. Zhou, and G. Hinds, Stress Corrosion Cracking of Steam Turbine Disc Steel—Measurement of the Crack-Tip Potential, *Corros. Sci.*, 2004, **46**(1), p 193–211
15. M. Mohtadi-Bonab, J. Szpunar, R. Basu, and M. Eskandari, The Mechanism of Failure by Hydrogen Induced Cracking in an Acidic Environment for API, 5L X70 Pipeline Steel, *Int. J. Hydrogen Energy*, 2015, **40**(2), p 1096–1107
16. Q. Yu and Y. Sun, The Pitting Behavior Research of X70 Pipeline Steel, *Mater. Heat Treat.*, 2010, **39**(2), p 1–3

17. M. Li, H. Lin, and C. Cao, Study on Soil Corrosion of Carbon Steel by Electrochemical Impedance Spectroscopy (EIS), *J. Chin. Soc. Corros. Prot.*, 2000, **20**(2), p 111–117

18. M. Jafarian, F. Gobal, I. Danaee, R. Biabani, and M. Mahjani, Electrochemical Studies of the Pitting Corrosion of Tin in Citric Acid Solution Containing Cl^-, *Electrochim. Acta*, 2008, **53**(13), p 4528–4536

19. P. Ernst and R. Newman, Pit Growth Studies in Stainless Steel Foils. II. Effect of Temperature, Chloride Concentration and Sulphate Addition, *Corros. Sci.*, 2002, **44**(5), p 943–954